Supporting Information

Dielectric metasurfaces for complete control of phase, amplitude and polarization

Tong Wu, Xueqian Zhang, Quan Xu, Eric Plum, Kaiji Chen, Yuehong Xu, Yongchang Lu, Huifang Zhang, Ziying Zhang, Xieyu Chen, Guanhua Ren, Li Niu, Zhen Tian, Jiaguang Han* and Weili Zhang**

1. Definition of transimission

The transmission in the main text happens at the meta-molecule interface, where the terahertz wave is transmitted from silicon across the meta-molecule into air, as illustrated in **Figure S1**. The corresponding transmission amplitude is defined by the square root of the transmittance at the interface, which is calculated by $|t| = |A_{air}/A_{Si}|/\sqrt{n_{Si}}$ with A_{air} and A_{Si} respectively representing the amplitude of the transmitted electric field in the air and the amplitude of the incident electric field in the silicon substrate, and n_{Si} representing the refractive index of silicon.

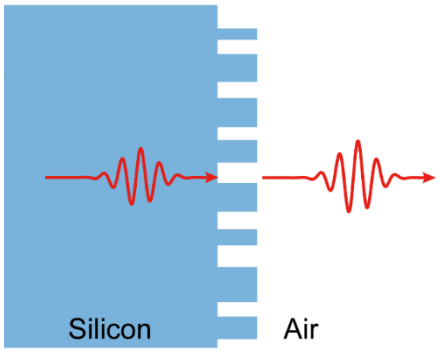

Figure S1. Schematic of transmission as defined in our manuscript. The terahertz wave is transmitted from silicon across the meta-molecule into air.

2. Completeness of the proposed meta-molecule database

To show the completeness of our meta-molecule database in controlling the phase, amplitude and polarization of THz waves, we first set up a series of standard sampling points to cover the polarization-dependent phase-amplitude space. Here, the amplitude is divided into 6 levels from 0 to 1 with 0.2 interval, while the phase is divided into 8 levels from 0° to 360° with 45° interval.

Hence, there are 6 × 8 × 6 × 8 = 2304 standard points covering the Ψ_x-$|t_x|$-Ψ_y-$|t_y|$ space. Then, we select the meta-molecule with response closest to these standard points from the corresponding structure databases. As mentioned in the main text, each meta-molecule is selected to provide the minimum error of $(|A_{tx}\exp(i\Psi_{tx}) - |t_x|\exp(i\Psi_x)| + |A_{ty}\exp(i\Psi_{ty}) - |t_y|\exp(i\Psi_y)|)_{min}$. At last, the completeness of our meta-molecule database is expressed by the amplitude of the minimum errors. The corresponding error distribution is shown in Figure S2, where the maximum error is 0.37 and the average error is only 0.13. For comparison, in many previous studies where sole phase control is applied, the phase is often divided into 8 levels with 45° interval[S1,S2]. This allows maximum ±22.5° phase deviation from the real requirement, corresponding to a maximum error of 0.39 ($|\exp(i\pi/8) - \exp(i\pi/4)|$). In those cases, the device performances were very good. Clearly, our design has smaller errors. Therefore, we consider our structure database to be complete. Meanwhile, we believe the error can be reduced further through smaller simulation intervals in changing D_{x1}, D_{y1}, D_{x2}, and D_{y2}.

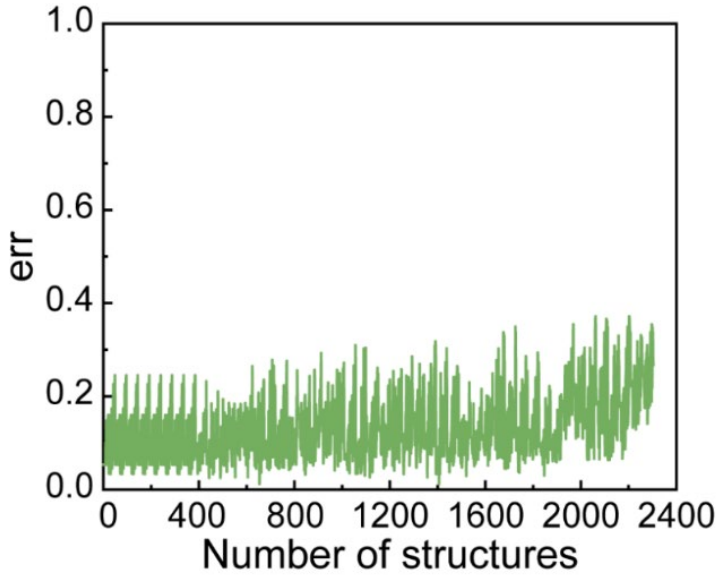

Figure S2. Calculated error distribution describing the difference in electromagnetic properties of the best-fitting meta-molecules from our meta-molecule database and 2304 sets of target properties based on standard sampling points.

3. The influence of meta-atom coupling on the meta-molecular response

To show the influence of coupling between meta-atoms on the total electromagnetic response of meta-molecules, we carried out numerical simulations on both far-field transmission and near-field distribution of two exemplary meta-molecules, as illustrated in **Figure S3**. Figure S3a illustrates one meta-molecule with D_{x1} = 30 μm, D_{y1} = 50 μm, D_{x2} = 50 μm, D_{y2} = 40 μm. Figure S3b shows the corresponding simulated transmission amplitude spectrum $|t_s|$ under *x*-polarized illumination alongside those of the two constituent meta-atoms $|t_1|$, $|t_2|$ obtained when there is only one meta-atom in a unit cell with a period of 110 μm, as well as the meta-molecule's calculated transmission amplitude spectrum $|t_c| = |t_1 + t_2|/2$ according to the interference model. It can be clearly seen that $|t_s|$ and $|t_c|$ are quite different. The complex amplitude error at 1.23 THz approaches 0.93. This indicates that the overall electromagnetic response of this meta-molecule is not solely determined by the individual electromagnetic responses of the two meta-atoms, and there is strong coupling effect between them.

To show the coupling effect, we plot *xz* and *xy* cross-sections of the simulated near-field distribution of the meta-molecule (as indicated by the green and orange planes in Figure S3a) in Figure S3c and S3d, respectively. In this case, both pillars have relatively strong leaky fields with clear field overlap, which causes the coupling effect and thus tailors the total electromagnetic response. Figure S3e to S3h illustrate the corresponding simulated results of another meta-molecule with D_{x1} = 70 μm, D_{y1} = 35 μm, D_{x2} = 60 μm, D_{y2} = 70 μm. In this case, $|t_s|$ and $|t_c|$ are quite close with the complex amplitude error only 0.012 at 1.23 THz, indicating a small coupling effect. This is verified by the simulated field distributions, where the fields are mainly confined inside the two pillars and even the leaky fields are well confined at their surfaces with nearly negligible field overlap.

The above two cases clearly demonstrate that coupling will affect the overall electromagnetic response of the meta-molecule, causing it to deviate from the interference

model. To achieve complete control, a huge number of meta-molecules are required to build a full meta-molecular database, thus it is hard to avoid the coupling effect through selecting enough meta-atoms with well-confined fields under both *x*- and *y*-polarized illumination. Therefore, we use massive simulations to build a meta-molecule database that takes coupling within meta-molecules into account and approximates coupling between meta-molecules by considering the response of a periodic structure. Effects due to different geometry of coupled meta-molecules are neglected.

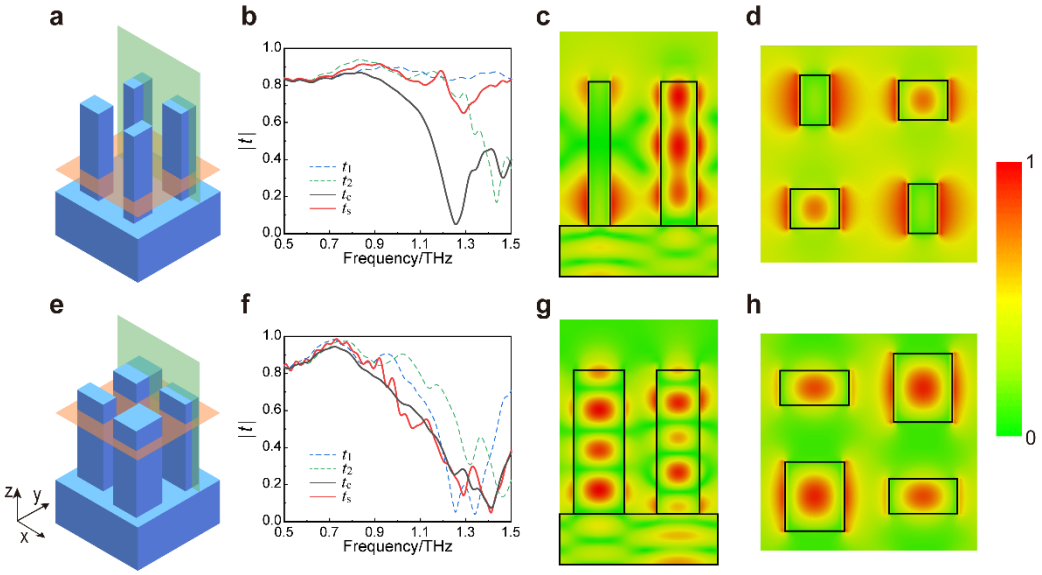

Figure S3. Influence of meta-atom coupling on the meta-molecular electromagnetic response. a,e Schematic of two meta-molecules with strong and weak internal coupling effects, respectively. **b,f** Simulated transmission amplitude spectra of the simulated meta-molecule $|t_s|$ and their constituent meta-atoms $|t_1|$, $|t_2|$, as well as that according to the interference model calculated by $|t_c| = |t_1 + t_2|/2$. **c,g** *xz* cross-sections and **d,h** *xy* cross-sections of simulated near-field distributions of the two meta-molecules, respectively. All results are shown for *x*-polarized illumination.

4. The error distributions of the designed meta-holograms

All the designed meta-holograms in the main text contain 45 × 45 = 2025 pixels. Their corresponding required amplitude and phase distributions are illustrated in Figure 2c,d, 3c-f, and 4c-f. To show how close the responses of our selected meta-molecules from the structure

database are to the required ones, we calculated the corresponding error distributions of the 2025 pixels in the three meta-holograms with the same method as in Supplementary Section 2, as illustrated in Figure S4. It can be seen that the polarization-independent meta-hologram has the smallest errors (average error 0.02, maximum error 0.07), see Figure S4a, which can be attributed to the larger meta-molecule density for such kinds of meta-molecules (2-μm geometric interval) within the database. The errors of the polarization-dependent and vectorial meta-holograms are also small, see Figure S4b (average error 0.08, maximum error 0.21) and S4c (average error 0.07, maximum error 0.20). The relatively larger error level for the latter two cases can be attributed to the smaller density of such meta-molecules (5-μm geometric interval) within the meta-molecule database. Such results guarantee that the designed meta-holograms can achieve good imaging performance.

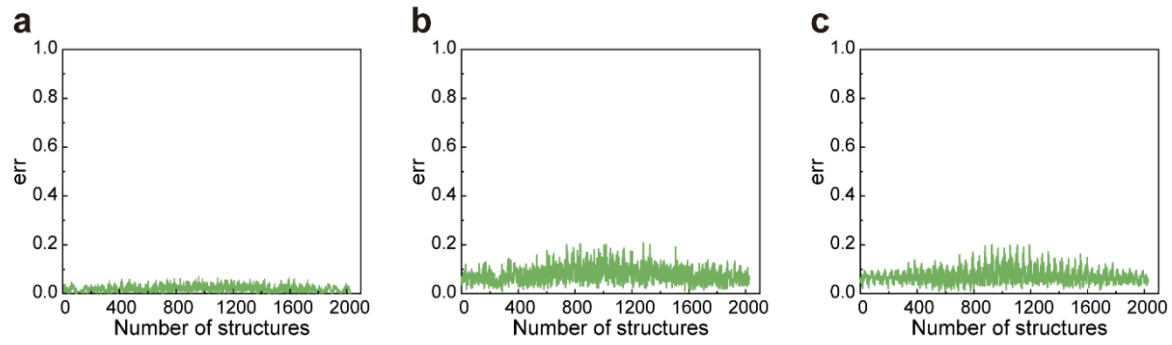

Figure S4. **a**-**c** Error distributions of the electromagnetic properties of the meta-molecules of the designed polarization-independent **a**, polarization-dependent **b**, and vectorial **c** meta-holograms compared to the corresponding ideal ones, respectively.

5. Meta-hologram performance with sole phase control

To show the importance of the simultaneous amplitude and phase control in designing meta-holograms, two more control meta-holograms are theoretically designed with sole phase control methods to generate a target holographic image of the letter “A”. One is designed by simply using the phase distribution in Figure 4d with homogeneous amplitude distribution (i.e. neglecting the corresponding amplitude distribution in Figure 4c), while the other is designed

using the conventional Gerchberg-Saxton iteration algorithm. The corresponding calculated intensity and phase distributions of the generated holographic image are illustrated in Figure S5. For the former meta-hologram, though the letter "A" can be recognized in the intensity distribution, the imaging performance is poor, see Figure S5a. Yet, the phase distribution shows fairly good imaging performance, see Figure S5b. For the latter meta-hologram, though the intensity distribution generates the letter "A" well, see Figure S5c, the corresponding phase distribution contains little image information, see Figure S5d. Such results can be attributed to the inadequacy of controlling phase but not amplitude.

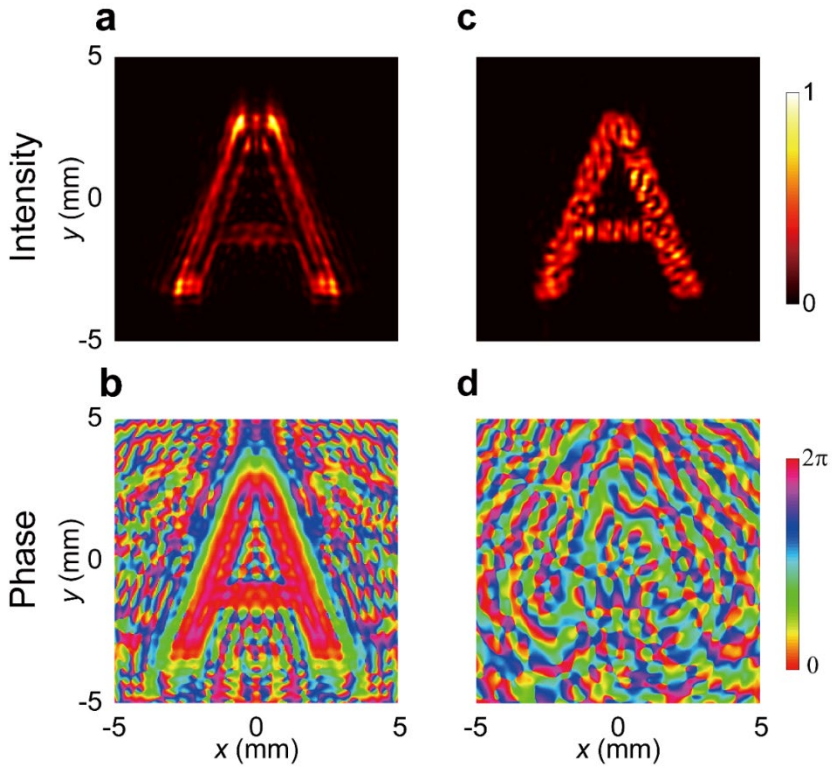

Figure S5. a-d Theoretical calculated intensity distributions **a**,**c** and phase distributions **b**,**d** of the generated holographic images from the meta-holograms designed using sole phase control methods, where **a**,**b** correspond to the meta-hologram designed by just considering the phase distribution in Figure 4d, and **c**,**d** correspond to the meta-hologram designed using the Gerchberg-Saxton iteration algorithm.

6. Imaging performance of the polarization-independent meta-hologram under different illuminating polarizations

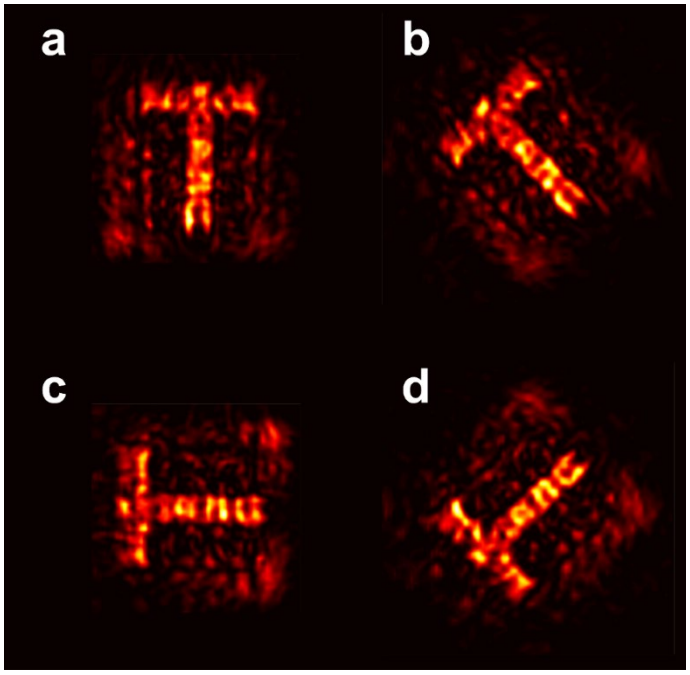

Figure S6. **a-d** Measured intensity distributions of the generated holographic image of the polarization-independent meta-hologram at 1.23 THz under *x*-polarized **a**, 45°-polarized **b**, *y*-polarized **c**, and −45°-polarized **d** illumination, respectively. In the measurements, we rotated the meta-hologram by 0°, 45°, 90°, and 135° instead of varying the incident and detected polarization states to achieve the desired illuminating polarizations.

7. Isotropic silicon antireflection metasurface

In the main text, the reflection at the flat and bare air-silicon interface at the other side of the silicon substrate is not considered, which in real cases will bring 30% reflection loss, as illustrated in **Figure S7**a. To reduce it, an antireflection film[S3] can be added on this interface. Here, to address this problem, an alternative solution, a silicon antireflection metasurface,[S4,S5] is presented, as illustrated in Figure S7b. Figure S7c illustrates the basic meta-atom design, which is a square-shape silicon pillar with side lengths $D_x = D_y$ =36.9 μm, height h = 32.3 μm and periods $P_x = P_y$ = 50 μm. Such an isotropic meta-atom design guarantees a polarization-independent response. The corresponding simulated reflectance R and transmittance T spectra

of the antireflection layer are illustrated in Figure S7d. It is seen that the reflectance (transmittance) at 1.23 THz is almost 0 (100%). Besides, the overall transmittance is over 94% in a broad frequency range from 1.0 to 1.5 THz.

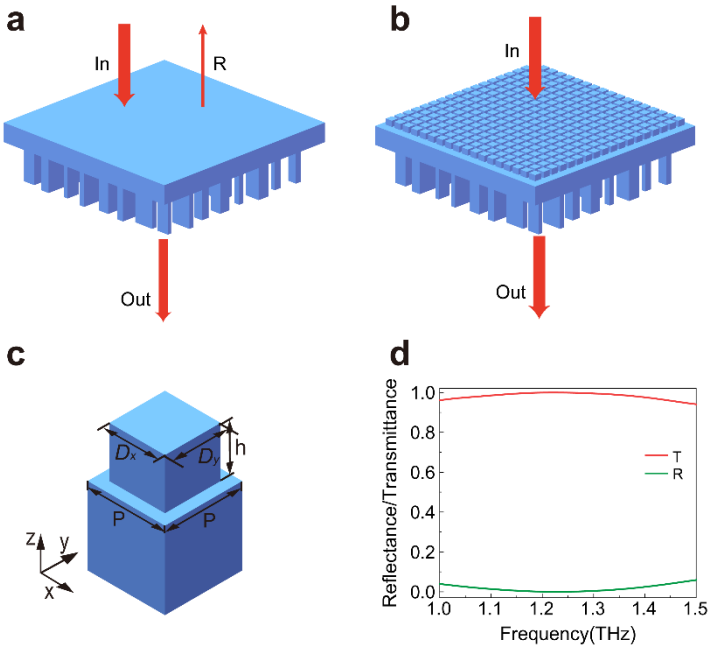

Figure S7. Antireflection metasurface schematics and performance. a Reflection loss at the bare air-silicon interface of the proposed meta-devices. **b** Meta-device with antireflection metasurface. **c** Designed silicon meta-atom. **d** Simulated transmittance and reflectance spectra of the antireflection silicon metasurface.

8. Working bandwidth of the meta-holograms

8.1 Working bandwidth of the polarization-independent meta-hologram

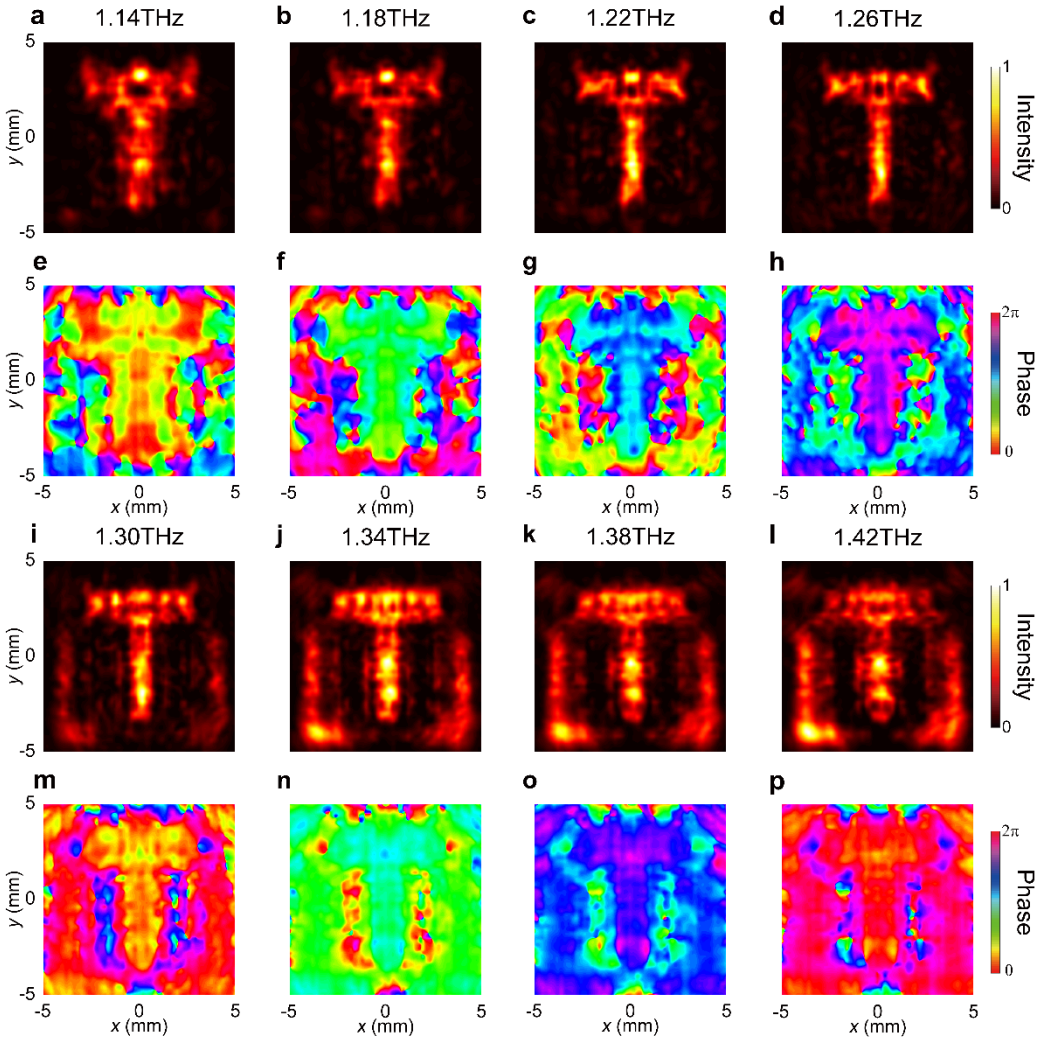

Figure S8. Measured *x*-polarized holographic results of the polarization-independent meta-hologram at different frequencies. Measured intensity **a-d, i-l** and phase **e-h, m-p** distributions of the holographic image from 1.14 to 1.42 THz with 0.04 THz steps. The effective working bandwidth is about 0.2 THz (1.18 to 1.38 THz).

8.2 Working bandwidth of the polarization-dependent meta-hologram

1) *x*-polarized illumination

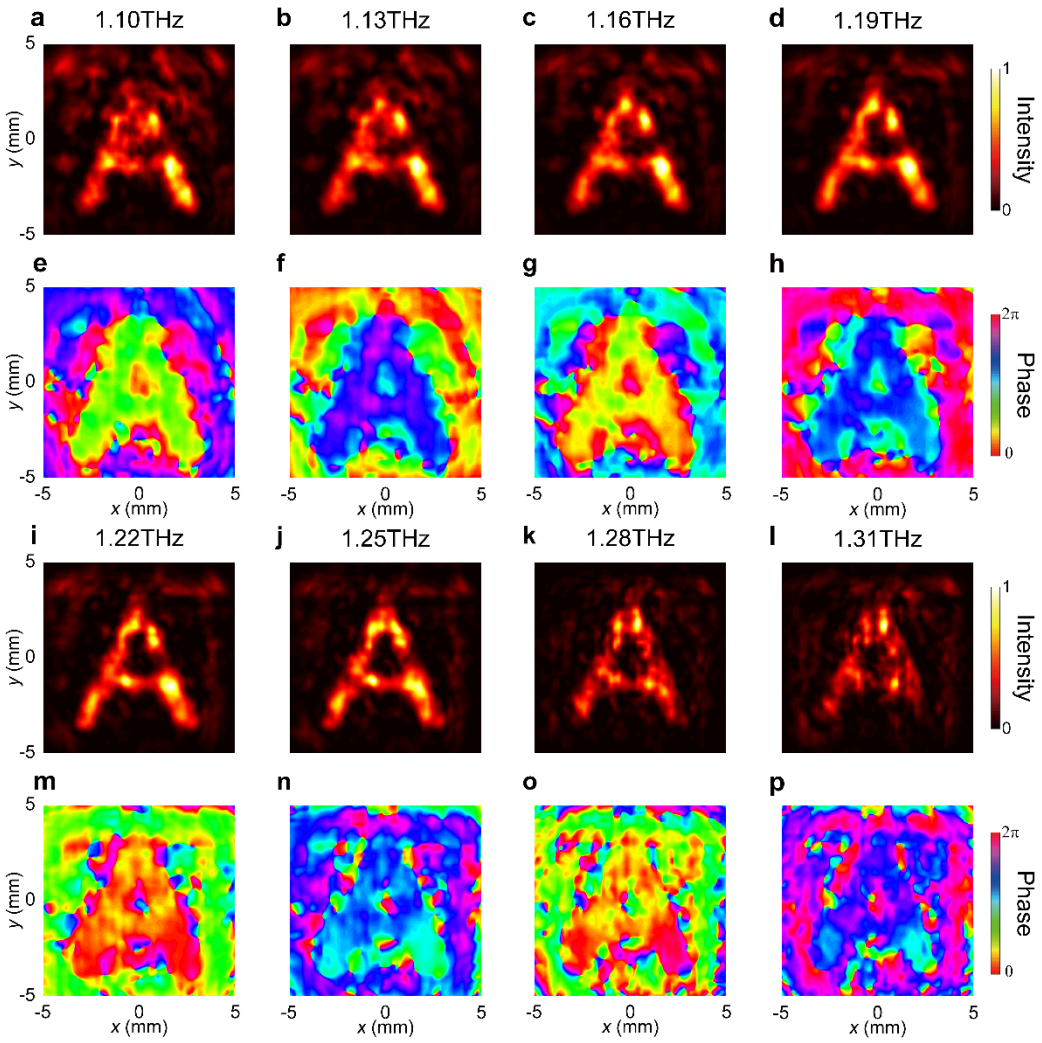

Figure S9. Measured *x*-polarized holographic results of the polarization-dependent meta-hologram at different frequencies. Measured intensity **a-d, i-l** and phase **e-h, m-p** distributions of the holographic image from 1.10 to 1.31 THz with 0.03 THz steps. The effective working bandwidth is about 0.15 THz (1.13 to 1.28 THz).

2) *y*-polarized illumination

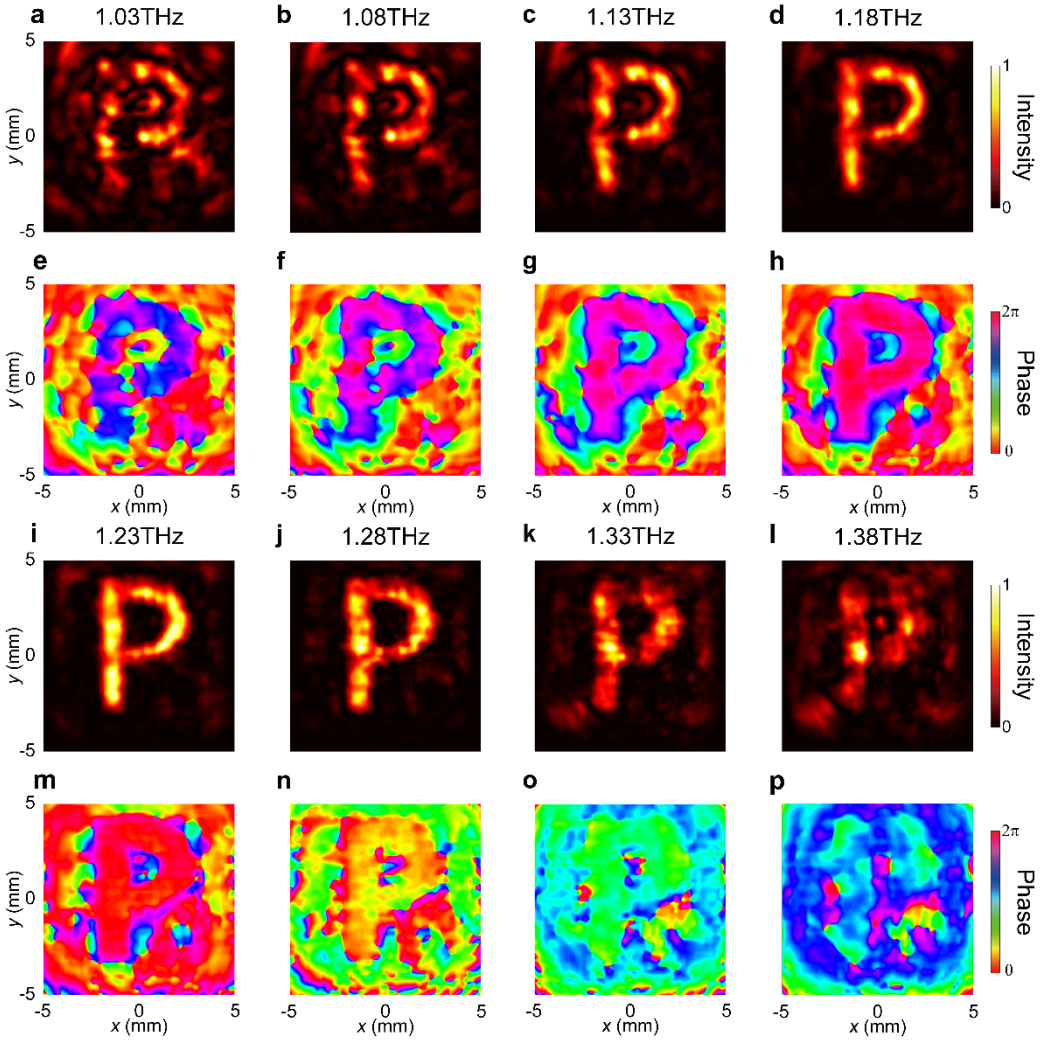

Figure S10. Measured *y*-polarized holographic results of the polarization-dependent meta-hologram at different frequencies. Measured intensity **a-d, i-l** and phase **e-h, m-p** distributions of the holographic image from 1.03 to 1.38 THz with 0.05 THz steps. The effective working bandwidth is about 0.25 THz (1.08 to 1.33 THz).

8.3 Working bandwidth of the vectorial meta-hologram

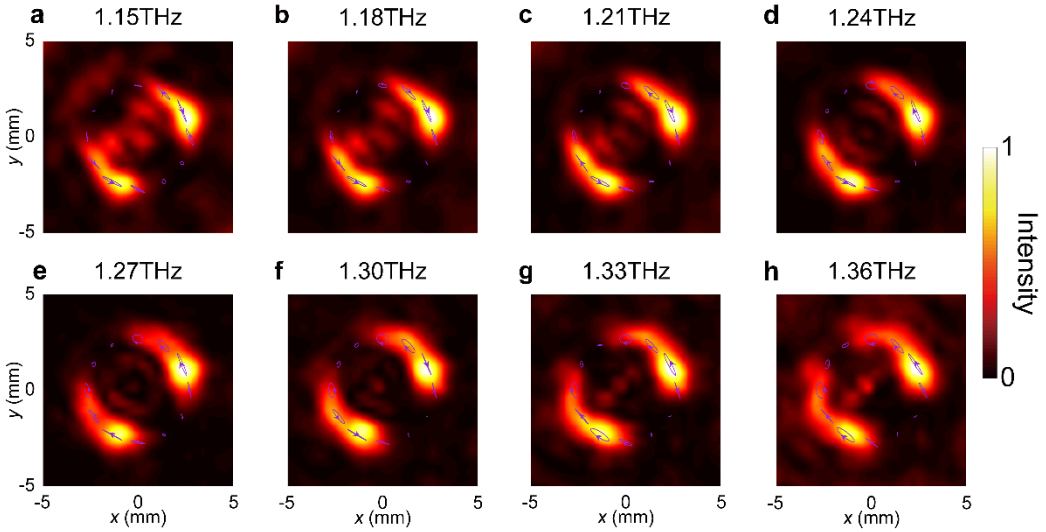

Figure S11. Measured holographic results of the vectorial meta-hologram at different frequencies. a-h Measured intensity distributions of the holographic image from 1.15 to 1.36 THz with 0.03 THz steps , respectively. The inset arrows along a ring depict the corresponding polarization distributions. The effective working bandwidth is about 0.15 THz (1.18 to 1.33 THz).

9. Arbitrary polarization generation

The transmission matrix of the designed meta-molecule in Figure 1a can be expressed as:

$$T = \begin{bmatrix} |t_x| e^{i\Psi_x} & 0 \\ 0 & |t_y| e^{i\Psi_y} \end{bmatrix}. \tag{S1}$$

Under an arbitrarily polarized incident wave with electric field of $E_{in} = [\sin\chi, \cos\chi e^{i\delta}]^T$, where $\chi \in [0, \pi/2]$ and $\delta \in [0, 2\pi]$, the output field can be calculated as:

$$E_{out} = TE_{in} = \begin{bmatrix} |t_x| \sin\chi e^{i\Psi_x} \\ |t_y| \cos\chi e^{i(\Psi_y+\delta)} \end{bmatrix} = A \begin{bmatrix} \frac{|t_x| \sin\chi}{A} \\ \frac{|t_y| \cos\chi}{A} e^{i(\Psi_y - \Psi_x + \delta)} \end{bmatrix} e^{i\Psi_x}, \tag{S2}$$

where $A = [(|t_x|\sin\chi)^2 + (|t_y|\cos\chi)^2]^{1/2}$ represents the amplitude, the Jones matrix at the right side represents the normalized output polarization state, and Ψ_x represents the overall output phase.

We have proven that our meta-molecule database allows complete control of $|t_x|$, Ψ_x, $|t_y|$, Ψ_y. Without loss of generality, we suppose $|t_x|$, $|t_y| \in [0, 1]$ and Ψ_x, $\Psi_y \in [0, 2\pi]$. Though the x- and y-polarized transmission amplitudes of our meta-molecule database cannot achieve unity, this can be obtained by carrying out self-normalization. Therefore, except for the cases of $\chi = 0$ and $\pi/2$ for the incident polarization, arbitrary polarization states can be generated with the amplitude range of $A \in [0, \{\sin\chi, \cos\chi\}_{\min}]$ and any overall phase within the full 2π range, thus allowing for vectorial meta-hologram designs.

10. Experiment setup

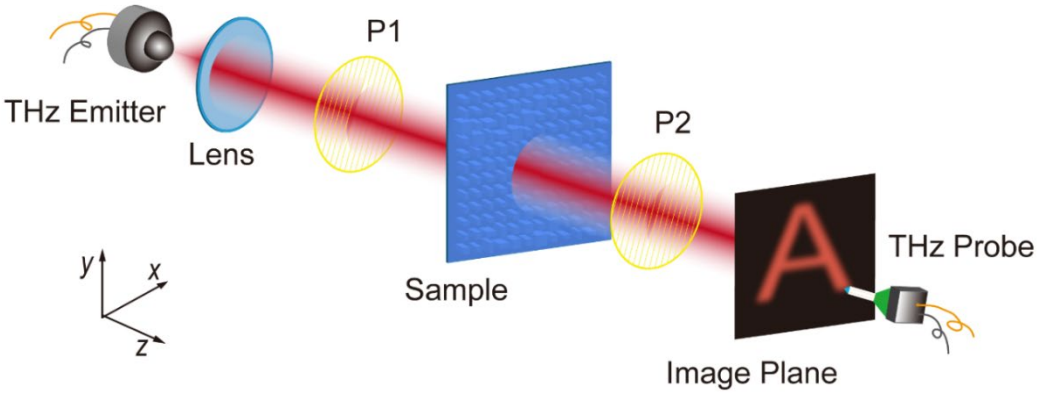

Figure S12. Schematic of the experimental setup for characterizing the meta-holograms. P1 and P2: polarizers.

References

[S1] N. Yu, P. Genevet, M. A. Kats, F. Aieta, J. P. Tetienne, F. Capasso, Z. Gaburro, *Science* **2011**, 334, 333.

[S2] H. Zhang, X. Zhang, Q. Xu, Q. Wang, Y. Xu, M. Wei, Y. Li, J. Gu, Z. Tian, C. Ouyang, X. Zhang, C. Hu, J. Han, W. Zhang, *Photonics Res.* **2017**, 6, 24.

[S3] A. J. Gatesman, J. Waldman, M. Ji, C. Musante, S. Yngvesson, *IEEE Microw. Guided Wave Lett*. **2000**, 10, 264.

[S4] H. Zhang, X. Zhang, Q. Xu, C. Tian, Q. Wang, Y. Xu, Y. Li, J. Gu, Z. Tian, C. Ouyang, X. Zhang, C. Hu, J. Han, W. Zhang, *Adv. Opt. Mater.* **2018**, 6, 1700773.

[S5] A. Cordaro, J. Groep, S. Raza, E. F. Pecora, F. Priolo, M. L. Brongersma, *ACS Photonics* **2019**, 6, 453.